Eur. Phys. J. B **3**, 73–82 (1998)

THE EUROPEAN PHYSICAL JOURNAL B

Polymorphism and chevron layer structure of an antiferroelectric liquid crystal studied by X-ray diffraction

P. Cluzeau[1,a], P. Barois[2], H.T. Nguyen[2], and C. Destrade[2,b]

[1] Laboratoire de Dynamique et Structure des Matériaux Moléculaires, Université de Lille 1, 59655 Villeneuve d'Ascq Cedex, France
[2] Centre de Recherche Paul Pascal, avenue A. Schweitzer, 33600 Pessac, France

Received: 13 November 1996 / Received in final form: 19 January 1997 / Accepted: 30 January 1998

Abstract. We report X-ray diffraction experiments performed on an antiferroelectric compound exhibiting a very rich polymorphism ($S_{I^*A}-S_{C^*A}-S_{C^*FI1}-S_{C^*FI2}-S_{C^*}-S_{C^*\alpha}-S_A$). The structural study of the unknown phases only allows us to exclude some phenomenological models. The use of oriented planar samples prepared between solid glass plates generate by cooling from the S_A phase a chevron structure of tilted layers already well characterized for the S_{C^*} phase. The extensive analysis of the evolution of the chevron structure through the numerous smectic-smectic phase transitions provides some original information in three distinct areas: fundamental data on the important physical parameters in the chevron structure formation, detection of the smectic-smectic phases transition by small change of the chevron structure, and information on the local molecular order induced by the alignment layer (interaction with a rubbed polymer).

PACS. 78.70.Ck X-ray scattering – 61.30.Jf Defects in liquid crystals – 64.70.Md Transitions in liquid crystals

1 Introduction

The subject of this experimental paper concerns both new chiral smectic phases and defects generated by the confinement ("chevron" layer structure). So, in the first part of the introduction we give a brief review of the actual knowledge required for a good understanding of our results.

In the last eight years much attention has been paid to chiral liquid crystals with the experimental discovery of the Twist Grain Boundary phase (TGB) by Goodby *et al.* [1] and the antiferroelectric smectic-C phase, initially called S_{O^*} by Levelut *et al.* [2], and then S_{C^*A} by Chandani *et al.* [3]. The studies of the TGB phases by X-ray diffraction have quickly revealed their structure [1,4]. Concerning the second type of chiral system, the situation is more complex. Indeed, the S_{C^*A} phase is generally accompanied by other "exotic" smectic phases. For example, in the most classical phase sequence [3,5,6]: $S_A-S_{C^*\alpha}-S_{C^*}-S_{C^*FI}-S_{C^*A}$, X-ray diffraction experiments cannot discriminate between the structure of the last four mesophases.

Nevertheless, the S_{C^*A} phase structure has been established by optical observations at the isotropic$-S_{C^*A}$ interface by Galerne *et al.* [7,8] and confirmed by X-ray diffraction experiments performed on oriented samples of racemic mixtures [2]. The properties under electric field of the $S_{C^*\alpha}$ and S_{C^*FI} (sometimes called subphases on account of their disappearance on racemic mixture [9]), respectively antiferroelectric and ferrielectric have given rise to numerous phenomenological models [10–18]; all are based on the competition between the ferroelectric and antiferroelectric order, but there is not yet experimental proof of their structure.

Interestingly, the studies of the ferro-, ferri-, and antiferroelectric phases are not only structural but also relevant for devices applications. These applications are possible owing to the Surface Stabilised Ferroelectric Liquid Crystal (SSFLC) cells, initially developed by Clark and Lagerwall [19] for the S_{C^*} phase. In this type of sample, the alignment of the molecules parallel to the glass substrate is generally obtained by interactions with a rubbed polymer. Concerning the orientations of the layers in the S_{C^*} phase, different experiments [20,21] have shown that the so-called "bookshelf" geometry (see Fig. 1a) in which the layers were assumed to be normal to the cell plates was inadequate [20]. The informations on the local layer structure (LLS) obtained by X-ray diffraction [20–23] and also by an analysis of the optical defects [24–26] have revealed

[a] e-mail: `cluzeau@lip5rx.univ-lille1.fr`

[b] Nous tenons à exprimer ici tout ce que nous devons à Christian Destrade récemment décédé ; il avait su nous communiquer son enthousiasme de longue date pour les propriétés fascinantes des nouvelles phases. C'est donc très humblement que nous lui dédions ce travail.

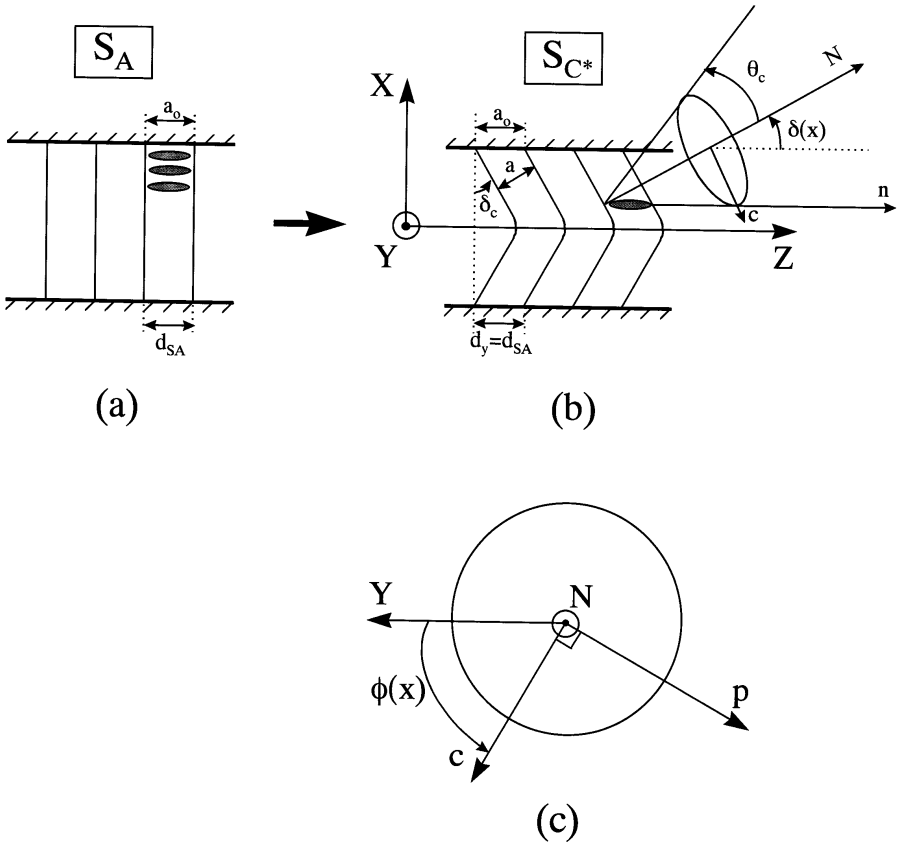

Fig. 1. In the cooling process of the cholesteric or isotropic phase, a "bookshelf" structure (a) can be formed in the S_A phase. After further cooling, the transition towards a S_{C^*} phase, or more generally towards a tilted smectic phase (molecules tilted relatively to the layers at an angle θ_C) induces a layer shrinking effect that is compensated by chevron formation (b). N is the layer normal, n the molecular director and c the c-director (the projection of the molecular director onto the smectic layer plane). This structure is characterized by a layer tilt angle $\delta(x)$ that varies between two values $-\delta_C$ and $+\delta_C$. It can also be formed directly if the S_A does not exist with $\delta_C \ll \theta_C$. In both cases, the layer tilt angle $\delta(x)$ is coupled with the molecular rotation (c) measured by the angle $\phi(x)$. p is the ferroelectric polarization.

a more complicated structure in which the tilted layers form a so called "chevron" (see Fig. 1b). In such a sample, the transition between the S_A and the S_{C^*} phase, or more generally, the decrease of the layer thickness, must induce an adjustment of the periodicity. Owing to the anchoring phenomena on the glass plate, the apparent thickness a_0 on the surface of the cell, and consequently the number of layers should remain unchanged. A possible way to accommodate the bulk and surface periodicity is to form the chevron structure suggested in Figure 1b, where the layer tilt effect compensates the effect of the molecular tilt. To explain the experimental results on the peculiar LLS (chevron structure) of the ferroelectric phase some phenomenological models have been developed [27–31]. In the first description of the chevron structure based on experimental results, Clark and Rieker [21] provide a simple explanation assuming the discontinuity of the c-director orientation as well as the layer structure at the chevron folding (see Figs. 1b and 1c). Nevertheless, such a discontinuity is somewhat in contradiction with the usual description of smectic elasticity. For that reason, the different phenomenological models are based on minimisation of the elastic free energy associated with dilatation, bending of the layer and rotation on the molecular smectic cone.

In the first step of this purely experimental work, we are looking for a possible specific diffraction feature and/or discontinuities in the evolution of the layer periodicity related to the numerous smectic-smectic phase transition.

In a second step, we analyse the evolution of the LLS through the different tilted smectic phases. The chevron structure behaviour in those new smectic phases is of great interest for the understanding of the predominant terms in the chevron formation or, the influence of the local molecular order: for example what happens to the boundary with the glass substrate for the c-director orientation in the S_{C^*A} phase?

Last, the extensive analysis of the LLS behaviour through the smectic-smectic phase transitions allows us to detect most of the phase transitions.

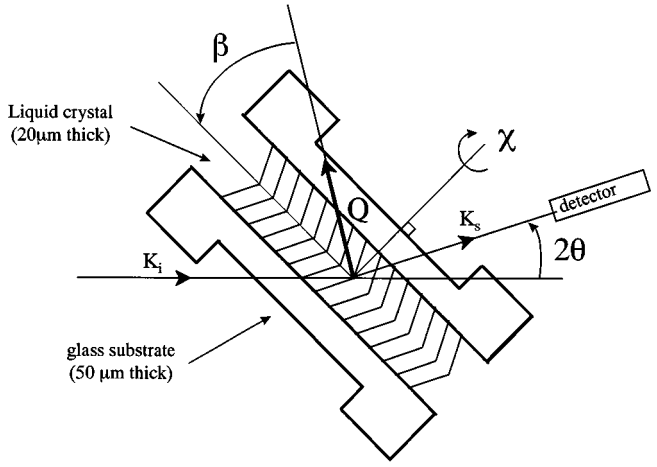

Fig. 2. The scattering geometry.

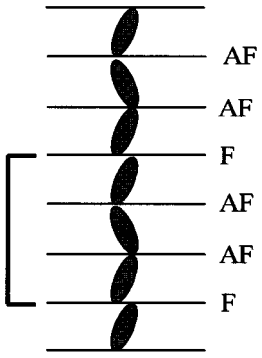

Fig. 3. One of the possible ferrielectric structure according to Isozaki *et al.* [13,14] based on competition between ferroelectric and antiferroelectric interactions.

2 Experimental

The compound used in this study is C8 tolane [5]. This material has already well characterised mesomorphic and electro-optic properties [5], dielectric studies [32]. It differs from MHPOBC by the tolane core and exhibits two ferrielectric phases.

The phase transition temperatures on heating according to DSC are the following [5] $S_{I^*A} - 71.6^\circ - S_{C^*A} - 95.1^\circ - S_{C^*FI1} - 96^\circ - S_{C^*FI2} - 97^\circ - S_{C^*} - 104^\circ - S_{C^*\alpha} - 105.5^\circ - S_A - 135.3^\circ - I$.

Nevertheless, as the two ferrielectric phases called S_{C^*FI1} and S_{C^*FI2} are not optically distinguishable on the planar samples used for this study, we will consider the $(S_{C^*FI1} + S_{C^*FI2})$ temperature range as a single ferrielectric phase called S_{C^*FI} [33].

The sample cells are prepared as shown in Figure 2. The material is confined between two ITO coated glass plates; the glass thickness is minimised to keep X-ray attenuation and scattering at negligible levels [4]. Uniform alignment of the director in the S_A phase is obtained with either rubbed polyimid or polyvinyl alcohol (PVA). For the cell prepared with polyimid the two plates are coated and rubbed, whereas for the cells prepared with PVA only one plate is coated and rubbed. A good alignment is achieved by very slow cooling through the isotropic to S_A phase transition. The alignment quality of all the samples is checked optically. The sample is mounted on a computer controlled Huber four circles diffractometer. The temperature is controlled with a 0.01 °C accuracy. The CuK_α radiation of a 18 kW rotating anode X-ray generator (Rigaku RU-200) is selected by a flat pyrolytic graphite (002) monochromator. The scattered X-ray intensity $I(\beta,\ \chi, 2\theta)$ is then function of the three variables β, χ, and 2θ, and is proportional to the local distribution of β, χ, and 2θ in the volume sampled by the X-ray beam (see Fig. 2).

First, the sample is rotated about the normal to the glass plane, χ in Figure 2, to bring the rubbing direction and therefore the Bragg wave vectors into the scattering plane. The angles 2θ and β can be now rocked at a set sample temperature to locate the Bragg peaks. The smectic layer spacing and the layer tilt angle can be then determined from the values of 2θ and β. Thus, this experiment provides as its output three distinct pieces of information: (1) the smectic layer spacing $d(T)$, where T is the temperature; (2) $I_\beta(\beta,\ 2\theta = 2\theta_{bragg})$ the probability distribution for the local orientation (β) of the smectic layer normal relative to an axis fixed to the cell (see Fig. 2); and (3) the evolution of $I_\beta(\beta)$ *versus* applied electric field at different temperatures. This last point will be discussed in a separate publication.

3 Results and discussion

3.1 Structural study of the unknown tilted smectic phases

In the S_{C^*A}, S_{C^*FI}, $S_{C^*\alpha}$ phases, X-ray diffraction experiments have shown that the smectic layer periodicity is smaller than the S_A layer periodicity confirming that in $S_{C^*\alpha}$ phase the molecules are tilted in the layer [34]. Nevertheless, we have to specify that in these small angle X-ray diffraction experiments the layer spacing and the direction of the molecular long axes are not measured independently. Consequently, the tilt angle values are deduced from the layer spacing, assuming that the tilt of the molecules is the unique factor that modifies the layer thickness (the molecular length is assumed to be temperature independent). Thus, in the following, these calculated tilt angle values will be called "apparent molecular tilt angle".

Moreover, we have searched for possible wave vectors corresponding to an other periodicity than the layer spacing; but in all these phases we observe only the wave vector corresponding to monolayer spacing (within the accuracy of our experiment $Iq_0/2$ is detectable only if $Iq_0/2 > 10^{-4} Iq_0$). The understanding of this experimental fact is obvious for the S_{C^*A} phase because this phase is made of single monomolecular S_{C^*} layers where the helical pitch is close to twice the layer periodicity, thus the layer interfaces are all identical. Consequently, a wave vector relative to the structural periodicity (two layers) of the S_{C^*A} phase cannot appear.

Concerning the S_{C^*FI} and $S_{C^*\alpha}$ phases, the absence of wave vector different from the layer spacing, should

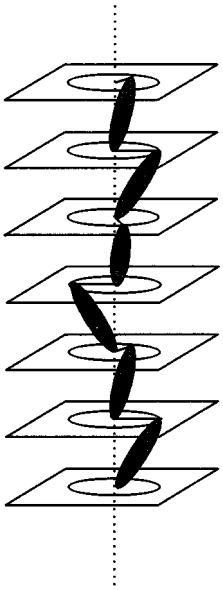

Fig. 4. One of the possible ferrielectric structure according to Lorman *et al.* [16] based on discrete variations of azimuthal angle.

indicate that some structural models are not valid. Indeed, two different types of model exist: the first one, developed by Japanese groups, is based on the juxtaposition of layers with ferroelectric and antiferroelectric ordering [13,14] (see Fig. 3), and the second type on the discrete variation of the azimutal angle [15–18]. An example is given by the so called "four layers" model (see Fig. 4) where the variation of the azimutal angle is 90° between two successive layers [16]. These two types of models, initially developed to account for the properties of the S_{C^*FI} phase, have been adjusted to the $S_{C^*\alpha}$ phase [13,18]; so, our analysis is valid indistinctly for these two phases.

From the X-ray experiments point of view, these structural models are both built with single molecular smectic layers of identical electronic density profile (same tilt angle). Nevertheless, the first type of model, sometimes called devil's staircase [13,14,35], give rise to different structures in which the layers interfaces are not all identical. For example, in Figure 3, every three layers, there is a ferroelectric layer interfaces; this periodicity should give rise to a superlattice visible in the X-ray diffraction experiments and characterised by a wave vector at $q_0/3$ (where q_0 is the single layer spacing wave vector).

The only way to keep the spirit of the devil's staircase model and the lack of superstructure periodicity should be to assume that the coexistence between ferroelectric and antiferroelectric order is purely statistic. The lack of wave vector different from q_0 can signify that the layer interfaces are identical. This experimental fact is in agreement with the second type of models [15,17].

3.2 Evolution of the layer thickness

The overall evolution of the layer thickness is given in Figure 5a. The layer spacing maximun value is about 39.25 Å in the S_A phase. It decreases abruptly at the $S_A-S_{C^*\alpha}$ phase transition, and then steadily throughout

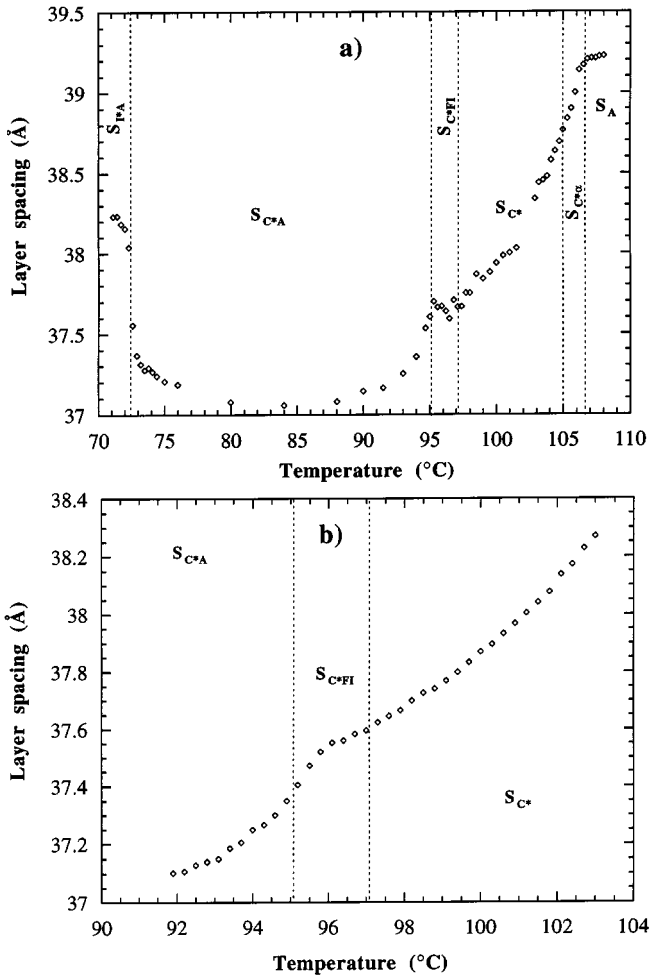

Fig. 5. (a) Layer spacing *versus* temperature between S_A and S_{I^*A} phase. (b) Layer spacing *versus* temperature for an other sample with better horizontal resolution.

the S_{C^*}, S_{C^*FI}, and S_{C^*A} phases to reach its minimum value at about 85 °C ($d = 37.05$ Å) in the S_{C^*A} phase. Finally, the smectic period increases abruptly on approaching the $S_{C^*A}-S_{I^*A}$ phase transition.

In summary, the evolution of layer spacing given in Figure 5a allows us to determine unambiguously the $S_A-S_{C^*\alpha}$ and the $S_{C^*A}-S_{I^*A}$ phase transitions; concerning the $S_{C^*}-S_{C^*FI}$ and $S_{C^*FI}-S_{C^*A}$ phase transition the resolution is too poor to draw useful conclusion (the accuracy is about ±0.1 Å). Thus, we have repeated the measurements between 92 °C and 103 °C with an improved resolution (the accuracy is now about ±0.025 Å). Interestingly, the curve clearly shows a break in the evolution of the layer thickness in the ferrielectric temperature range (see Fig. 5b). We have to specify that in Figures 5a and 5b the $S_{C^*}-S_{C^*FI}$ and $S_{C^*FI}-S_{C^*A}$ phase transitions temperature are given according to Differential Scanning Calorimetry. These temperatures are supplied for information only, knowing that these phase transitions are very dependent on sample thickness in planar geometry [33].

Nevertheless, we can notice that the measured layer spacing in the S_{C^*A} phase would not coincide with

the extrapolation from the behaviour in the S_{C^*} phase. The measured values in the S_{C^*A} phase are smaller than the extrapolated values. The same behaviour has been already observed on the racemic compound MHPOBC [36]. This experimental fact suggests a coupling between the tilt angle and the onset of the antiferroelectric ordering.

3.3 Chevron layer structure

3.3.1 Chevron layer structure formation

Most of the previous studies on chevron layer structure concerned the unwound S_{C^*} phase [20–23]. This is probably the reason why the orientation of the *c*-director (defined in Fig. 1c) on the glass substrate and at the chevron interface plane has been at first considered as the main parameter to explain the chevron formation. In our study, two new parameters arise: the first one already mentioned above is the helical structure in the bulk [5,37]; the second one is the existence of a local molecular order different from ferroelectric one (antiferroelectric or ferrielectric order).

In this paragraph, owing to the analysis of the evolution of the scattered intensity $I_\beta(\beta)$ *versus* β with the temperature and for different samples, we obtain information on the appearance of chevron structure and on the detection of some phase transition. Indeed, the scattered X-ray intensity is proportional to the local distribution of β in the volume sampled by the X-ray beam.

Figure 6a shows the evolution of $I_\beta(\beta)$ *versus* β through the $S_A-S_{C^*\alpha}$ phase transition. These experimental results are obtained with a 23 μm thick sample coated with rubbed PVA.

In the S_A phase, the peak is centered around $\beta = 0$, with a half height width $\Delta\beta$ of about 7°. The origin $\beta = 0$ is chosen along the normal to the glass plates (with an accuracy of ±1°). When the temperature decreases, we observe a broadening of the peak's base (see Fig. 6a at $T = 105.4$ °C) with the appearance of two small satellite peaks. At $T = 105.1$ °C, the intensity distribution is equally shared between three peaks. These three peaks can be explained either by the coexistence of "bookshelf" structure with chevron structure area or by three chevron branches in the bulk. The last hypothesis seems to be confirmed by two experimental facts: the phase dependence of the third peak (for example, this peak vanishes at the $S_{I^*A}-S_{C^*A}$ phase transition on heating) and by the asymmetric chevron structure behaviour (see detail analysis in Sect. 3.3.2).

Moreover, the high minima values between the peaks is the signature of a continuous evolution of the layers bend between the chevron branches.

When the temperature still decreases, the chevron branches become well defined (see Fig. 6b), and the layer tilt angle corresponding to each chevron branch δ_{C+} and δ_{C-} is given by the angular position of the positive and the negative apex peaks. The peaks in $I_\beta(\beta)$ are rather sharp, having a half height width $\Delta\beta$ of about 1.5° at the temperature of $T = 98.8$ °C; $\Delta\beta$ decreases progressively with

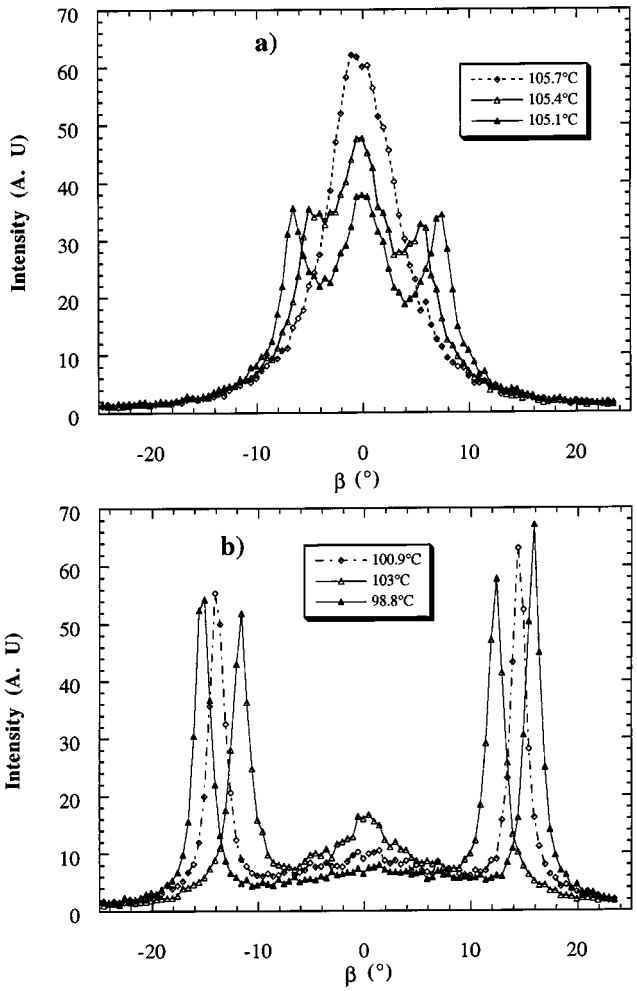

Fig. 6. (a) Evolution of the scattered intensity $I_\beta(\beta)$ *versus* β around the $S_A-S_{C^*\alpha}$ phase transition at $T = 105.7/105.4/105.1$ °C (23 μm thick sample coated with PVA). (b) evolution of the scattered intensity $I_\beta(\beta)$ *versus* β in the S_{C^*} phase, on decreasing temperature at $T = 103/100.9/98.8$ °C.

the temperature ($\Delta\beta_{103\ ^\circ C} = 1.8°$; $\Delta\beta_{100.9\ ^\circ C} = 1.6°$; $\Delta\beta_{98.8\ ^\circ C} = 1.5°$). Nevertheless, even far from the S_A phase transition the intensity level between the two peaks remains always different from zero; this experimental fact suggests a continuity of the layer owing to a bend at the chevron folding. Indeed, the characteristic length of the layer bend at the chevron folding decreases when the layer tilt increases as already predicted in phenomenological models [28,31].

3.3.2 Symmetric or asymmetric chevron layer structure

In the previous paragraph, we have described the appearance of what we called the "symmetric" chevron structure. The chevron structure is called "symmetric" when the chevron arms lengths are approximately equal. In this case, the layers in the S_A phase are quite normal to the glass substrate (with $\delta_A < 4$). These symmetric LLS

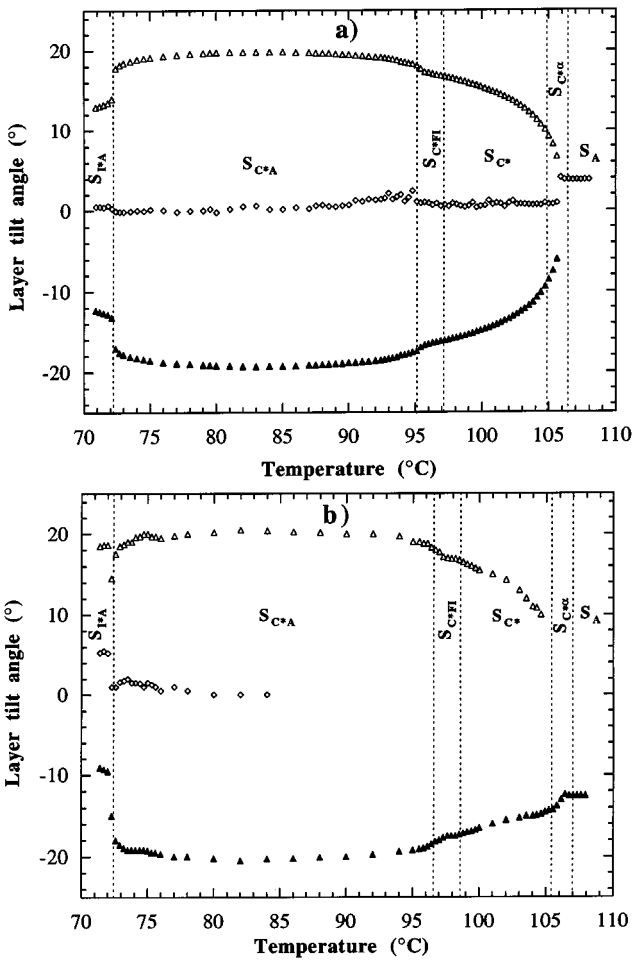

Fig. 7. (a) The layer tilt angle as a function of temperature obtained from the peak location in the $I_\beta(\beta)$ data; the layer tilt angle in the S_A phase is less than 4 degrees. This symmetric chevron structure is obtained with a 23 μm thick sample coated with PVA. (b) The layer tilt angle is about 13 degrees. This asymmetric chevron structure is obtained with a 20 μm thick sample coated with polyimid. We can notice the third peak which appears in the S_{C^*A} phase and is located at $\delta = 0$.

scenario are obtained in the samples with only one plate coated with PVA; this LLS behaviour is perfectly reproducible since it has been observed with three different samples.

The asymmetric LLS scenario, occurs with a sample where the two glass plates are coated and rubbed with polyimid: the layers are already tilted in the S_A phase ($\delta_A \approx 13°$) and the chevron arms length will not be equal in the tilted smectic phases.

It must be emphasized that even in the asymmetric LLS scenario, the layer tilt angles $\delta_{C-}(T)$ and $\delta_{C+}(T)$ are almost identical for both branches at a given temperature. The fitting of the scattered intensity $I_\beta(\beta)$ *versus* β at each temperature gives the local orientation (β) of the chevron branches and allows us to plot the layer tilt angle $\delta(T)$ as a function of the temperature in the symmetric and asymmetric cases (see Figs. 7a and 7b).

Moreover, in both cases (symmetric and asymmetric), there is a small broad peak centred on $\beta = 0$ in the tilted smectic phases. The interpretation of this peak (given in the previous section) as a short section roughly perpendicular to the glass plates is yet questionable. Indeed, one could argue that the relatively large area (1×2 mm^2) of the X-ray beam always illuminates a zig zag wall defect; the zig zag defect contains layers normal to the glass plates which could give rise to some intensity scattered at $\beta = 0$. But the conclusive argument is provided by the evolution of the asymmetric chevron structure *versus* temperature: a broad peak centred at $\beta = 0$ appears in the S_{C^*A} phase even though the layers are tilted of about 13° in the S_A phase. Consequently, the two main chevron branches tilted by δ_C are well linked up by a short section roughly perpendicular to the glass plates. The physical origin of these different behaviours between samples coated with PVA (δ_A weak) and polyimid ($\delta_A \approx 13°$) is probably linked to the high pretilt value induced by the polyimid. Indeed, the comparison of various associations of Liquid Crystal/alignment layer performed on nematic phases has shown a higher value of pretilt with polyimid than with other alignment layers [38].

We have now studied the intensity asymmetry of the peaks: when the intensity distribution is shared between two peaks with an intensity level truely equal to zero between the peaks, we are in presence of an ideal chevron structure firstly described by Rieker *et al.* [20]. In this approximation these authors have shown that the ratio of the intensity of the peaks (I_+/I_-) is proportional to the ratio of the chevron branches lengths (b_+/b_-). Thus, geometrical considerations in the triangle ABC (see Fig. 8) lead to the relation:

$$\frac{I_+}{I_-} = \frac{\tan\delta_C + \tan\delta_A}{\tan\delta_C - \tan\delta_A}.$$

Let us plot on the same graph $\frac{I_+}{I_-}$ and $\frac{\tan\delta_C + \tan\delta_A}{\tan\delta_C - \tan\delta_A} = R$ as a function of the temperature (see Fig. 9). The overall agreement between these two curves is rather good since the value of δ_A calculated from I_+, I_-, and δ_C in the S_{C^*} phase is about 4.4° while the experimental value of δ_A is about 4°. We have chosen to apply this relation to the symmetric chevron structure because of the weak intensity level between the peaks δ_{C+} and δ_{C-}. Surprisingly, the agreement decreases abruptly around $T = 95$ °C and becomes poor below this temperature; this behaviour is related to the increase of the intensity level around zero. A detailed analysis of the physical meaning of the intensity level variations on each chevron branch is presented in the next section.

3.3.3 Study of normalised intensity scattered from each chevron branch

All the results discussed in the previous Sections (3.1 and 3.2) have revealed only one singularity, a break in between the S_{C^*} and S_{C^*A} phase transition which is probably induced by a phase transition. To obtain more information

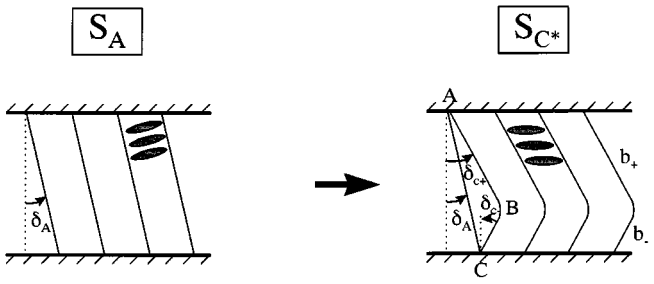

Fig. 8. δ_{A} is the layer tilt angle in the S_A phase. δ_{C+} and δ_{C-} are the layer tilt angle in the smectic tilted phases (in first approximation $\delta_{C+} = \delta_{C-}$); b_+ is the length of the longest chevron branch, b_- the length of the shortest one.

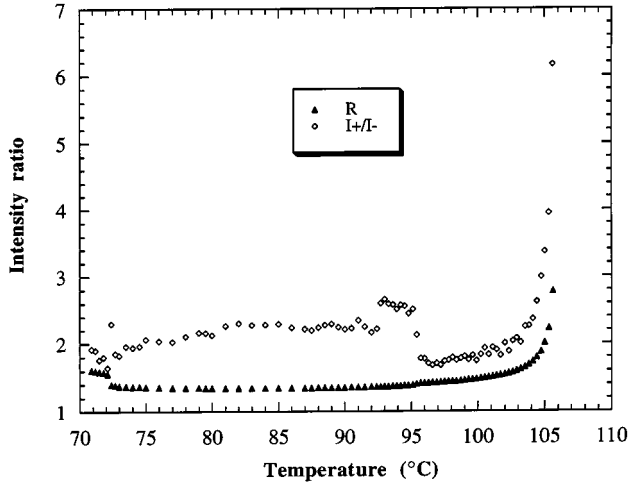

Fig. 9. Evolution of $\frac{I_+}{I_-}$ and $\frac{\tan\delta_C+\tan\delta_A}{\tan\delta_C-\tan\delta_A} = R$ *versus* temperature for the 23 μm thick sample coated with PVA. I_+ and I_- are the intensity values corresponding to each chevron branch obtained by fitting of $I_\beta(\beta)$ *versus* (β); δ_{A} is the layer tilt angle in the S_A phase and δ_C is the layer tilt angle in the tilted smectic phases at a given temperature.

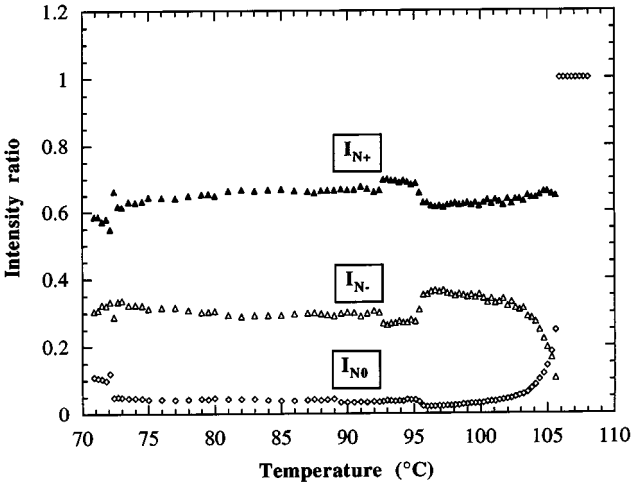

Fig. 10. Normalised intensity relative to each chevron branch *versus* temperature obtained by fitting of $I_\beta(\beta)$ *versus* (β): $I_{N_-} = I_-/(I_- + I_0 + I_+)$; $I_{N0} = I_0/(I_- + I_0 + I_+)$; $I_{N_+} = I_+/(I_- + I_0 + I_+)$ for the 23 μm thick sample coated with PVA.

on the other phase transition we have fitted $I_\beta(\beta)$ *versus* β and analysed the evolution of normalised intensity $\{I_{N_-} = I_-/(I_- + I_0 + I_+)$; $I_{N0} = I_0/(I_- + I_0 + I_+)$; $I_{N_+} = I_+/(I_- + I_0 + I_+)\}$ corresponding to each chevron branch (see Fig. 10). Interestingly, the plot of $I_N = f(T)$ reveals two breaks in the evolution of I_{N_+} and I_{N_-}, respectively at $T = 95.3$ °C and $T = 92.6$ °C. Theses breaks were also visible on the plot $\frac{I_+}{I_-} = f(T)$ in Figure 9. As the normalised intensity is directly proportional to the chevron arm length, the breaks in the curves correspond to sudden change in the chevron arm length. Such a rearrangement of the chevron structure is necessarily connected to a phase transition: the helical pitch divergence at the boundaries of the S_{C^*FI} phase [5] are probably responsible of these small changes of the relative chevron arm length. Then, we must explain why these modifications occur at temperatures which are shifted of about 2 °C from the transition temperatures measured by DSC. Two explanations are possible. Either, the strain due to the phase transition generates a rearrangement of the chevron branches only 2 °C below the phase transition, or the S_{C^*FI} phase transition temperatures are shifted of about 2 °C due to polar interaction with the rubbed polymers. As another study has shown that polar interaction between molecules and rubbed polymer favours ferroelectric phase [39]; the explanation by a shift of the transition temperatures of S_{C^*FI} phase will be retained.

Moreover, the evolution of $I_{N0} = f(T)$ reveals interesting behaviours:

- Firstly, we observe a decrease in the characteristic length of the layer bend at the chevron folding when the layer tilt increase which agrees well with phenomenological models [28,31].
- Secondly, the relative intensity I_{N0} is increased two fold at $T = 95.3$ °C and stays at this level down to $T = 72$ °C; this steep increase of the characteristic length of the layer bend is perfectly compatible with the $S_{C^*} - S_{C^*FI}$ phase transition, and its higher number of defects [40].

3.3.4 Comparison of apparent molecular tilt angle and chevron layer tilt angle

In Figure 11, the plot on the same graph of the temperature dependence of the apparent molecular tilt angle

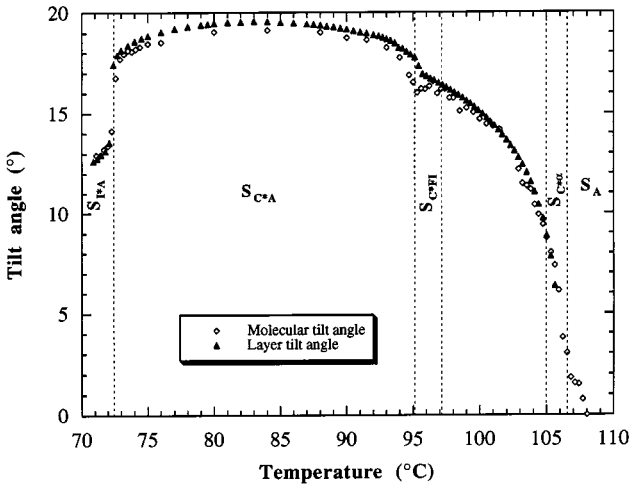

Fig. 11. Evolution of apparent molecular tilted angle (θ_{ap}) calculated from the layer thickness in the S_A phase, and of the layer tilt angle (δ_C) *versus* temperature for the 23 μm thick sample coated with PVA.

($\theta(T)$), already defined in Section 3.1., and of the layer tilt angle ($\delta(T)$) reveals two main informations (sample coated with PVA, 23 μm thick).

Firstly, it is obvious that the break in the ferrielectric temperature range occurs at the same temperature for the molecular tilt angle and for the layer tilt angle. As it has been already mentioned in Section 3.2, it is difficult to infer from Figure 11 whether the break occurs in the S_{C^*FI} phase, or at the $S_{C^*FI}-S_{C^*A}$ phase transition, or even at the $S_{C^*}-S_{C^*FI}$ phase transition because these phase transitions are dependent on sample thickness or even on the sample history. Nevertheless, the results of the previous section suggest that the break in the chevron layer and molecular tilt angles correspond to the $S_{C^*}-S_{C^*FI}$ phase transition.

Secondly, there is a quite perfect matching between the evolution of $\theta(T)$ and $\delta(T)$ considering the experimental uncertainty. In the previous studies on chevron structure with the $S_A-S_{C^*}$ phase transition, the layer tilt angle $\delta(T)$ is found smaller than the apparent molecular tilt angle $\theta(T)$, with for example $\delta(T) = 0.85\theta(T)$ according to Clark *et al.* [21]. In their study, the ratio $\delta(T)/\theta(T)$ is smaller than unity; this experimental fact could be explained when assuming that the layer spacing induced by the substrate has its own temperature dependence ($d_y(T) \neq d_{SA}$, see Fig. 1a). Whatever the physical origin of $\delta(T) < \theta(T)$, it implies that the molecules are not parallel to the z-axis and consequently the c-director position is different from $\pi/2$ (see Fig. 1).

In our case, as $\delta(T) \approx \theta(T)$ in the different tilted smectic phases, the molecules are necessarily parallel to the z-axis in the ferroelectric phase (c-director position equal to $\pi/2$). Consequently the local molecular antiferroelectric (or ferrielectric) order should be violated on (and near) the substrate in the antiferroelectric (or ferrielectric) phase because the polarisation direction (parallel to the y-axis) is imposed by the c-director position equal to $\pi/2$. Nevertheless, this violation of the molecular antiferroelectric order is in agreement with other optic and electro-optic results: for example, as already mentioned, the S_{C^*FI} and S_{C^*A} phases temperature ranges are very dependent on sample thickness. When the sample thickness decreases these phases are progressively replaced by S_{C^*} phase; or yet, the electro-optic behaviour of the S_{C^*A} phase is extremely dependent on sample thickness because of the ferroelectric order near the glass substrate [33,41]. Generally speaking, the alignment quality is poorer in the S_{C^*A} (or S_{C^*FI}) phase than in S_{C^*} phase whatever the polymer used for the sample preparation. This fact is also in good agreement with the persistence of a ferroelectric order near the substrate while the bulk is antiferroelectric (or ferrielectric). This vertical competition between ferroelectric and antiferroelectric (or ferrielectric) orders probably explains the highest number of defects in these phases [40].

4 Conclusion

Our experimental study provides some original information, at least, in four distinct fields: (1) structural information on the unknown phases; (2) important physical parameters in the chevron formation; (3) detection of the phase transitions by analysis of the chevron structure behaviour through the phase transitions; (4) information on the local molecular order induced by the substrate.

(1) In all the tilted smectic phases, a single wave vector (q_0) is observed. It corresponds to monolayer spacing. This lack of superstructure is compatible only with the phenomenological models where the ferrielectricity is described by discrete variation of the azimutal angle [15–18].

(2) The second category of results provides some answers on the important parameters in the chevron structure formation and behaviour. Figure 12 summarizes the relationship between the intensity profile ($I_\beta(\beta)$ *versus* β) and the chevron structure. The chevron structure formation starts with a simple bend of the layers just below the $S_A-S_{C^*\alpha}$ phase transition; on cooling, this layer bend is progressively confined into the middle of the sample. The intensity level different from zero between the peaks is unambiguously the signature of this layer bend (see Fig. 12b). Moreover, we have shown that a third peak centered on zero exists in some of the tilted phases (see Fig. 12c). Some experimental results prove that this peak is not due to zig zag wall defects (see Sect. 3.3.1 and 3.3.2.). At last, the good matching of $\delta(T)$ and $\theta(T)$ shows a perfect adjustment of the periodicity between the natural layer thickness in the bulk and that imposed at the boundaries. This set of experimental evidences suggests that the layer tilt angle is completely independent of the helical structure (all the tilted phases have an helical structure) and of the local molecular structure (antiferroelectric, ferrielectric, ferroelectric) confirming that the origin of the chevron layer structure is mainly related to the layer distortion energy rather than the c-director deformation energy [28,31].

(3) On this compound exhibiting numerous smectic-smectic phases transition, the analysis of the variation of

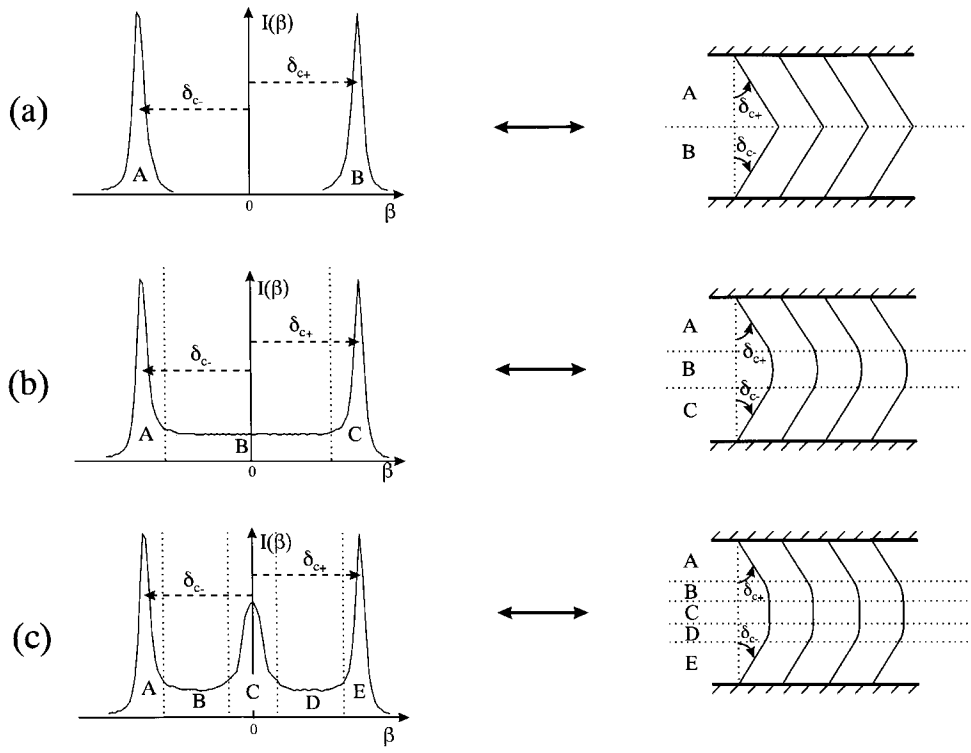

Fig. 12. Schematic illustration of the relationship between the intensity profile $I_\beta(\beta)$ *versus* β and the chevron structure. (a) The intensity profile exhibits two peaks (A and B) corresponding to the chevron arms A and B respectively tilted by δ_{C-} and δ_{C+} ($\delta_{C-} \approx \delta_{C+}$). The intensity level is equal to zero between the peaks: this case corresponds to a "perfect" chevron structure observed by Rieker *et al.* [20]. Such a chevron structure assumes a discontinuity of the layers (and of the *c*-director orientation) in the middle plane of the sample (in our experimental results we have never observed this case). (b) When the intensity level remains different from zero between the peaks the layer continuity is realized by a layer bend in the middle plane of the sample (area B). (c) The intensity profile exhibits now three peaks; the additional peak (C) centered on zero is relative to a third chevron arm roughly normal to the substrate. The intensity level different from zero between the three peaks corresponds also to a layer bend between the three chevron arms.

the chevron length reveals that a phase transition can induce a relative variation of the chevron arm length. This original result shows that even if the layer tilt angle is completely determined by the layer spacing, some of the characteristics of the chevron structure can be modified by other parameters, such as a strong pitch variation or a change in the local molecular order.

(4) Lastly, this study confirms a violation of the antiferroelectric and ferrielectric molecular order near the alignment layer already suggested by other experiments [33,41]. Indeed, the molecules look parallel to the z-axis (c-director position equal to $\pi/2$) which means that the local molecular order induced by the substrate is always ferroelectric.

We are grateful to Dr L. Limat and Dr M. Brunet for helpful discussion and to Dr C. Carboni and Pr G. Joly for critically reading the manuscript and making several useful remarks.

References

1. J.W. Goodby, M.A. Waugh, S.M. Stein, E. Chin, R. Pindak, J.S. Patel, Nature (London) **337**, 449 (1987).
2. A.M. Levelut, C. Germain, P. Keller, L. Liebert, J. Billard, J. Phys. France **44**, 623 (1983).
3. A.D.L. Chandani, Y. Ouchi, H. Takezoe, A. Fukuda, K. Furukawa, A. Kishi, Jpn. J. Appl. Phys. **28**, 1261 (1989).
4. L. Navailles, P. Barois, H.T. Nguyen, Phys. Rev. Lett. **71** 545 (1993).
5. P. Cluzeau, H.T. Nguyen, C. Destrade, N. Isaert, P. Barois, A. Babeau, Mol. Cryst. Liq. Cryst. **260**, 69 (1995).
6. H.T. Nguyen, J.C. Rouillon, P. Cluzeau, G. Sigaud, C. Destrade, N. Isaert, Liq. Cryst. **17**, 571 (1994).
7. Y. Galerne, L. Liebert, Phys. Rev. Lett. **64**, 906 (1990).
8. Y. Galerne, L. Liebert, Phys. Rev. Lett. **66**, 2891 (1991).
9. T. Isozaki, T. Fujikawa, H. Takezoe, A. Fukuda, T. Hagiwara, Y. Suzuki, I. Kawamura, Jpn. J. Appl. Phys. **31**, L1435 (1992).
10. K. Hiraoka, A. Taguchi, Y. Ouchi, H. Takezoe, A. Fukuda, Jpn. J. Appl. Phys. **29**, 103 (1990).
11. E. Gorecka, A.D.L. Chandani, Y. Ouchi, H. Takezoe, A. Fukuda, Jpn. J. Appl. Phys. **29**, 131 (1990).
12. J. Lee, A.D.L. Chandani, K. Itoh, Y. Ouchi, H. Takezoe, A. Fukuda, Jpn. J. Appl. Phys. **29**, 1122 (1990).
13. T. Isozaki, K. Fujikawa, H. Takezoe, A. Fukuda, Phys. Rev. B **48**, 121 (1993).
14. T. Isozaki, K. Ishikawa, H. Takezoe, A. Fukuda, Ferroelectrics **147**, 121 (1993).

15. H. Orihara, Y. Ishibashi, Jpn. J. Appl. Phys. **29**, L155 (1990).
16. V.L. Lorman, Liq. Cryst. **20**, 267 (1996).
17. V.L. Lorman, Mol. Cryst. Liq. Cryst. **262**, 437 (1995).
18. M. Cepic, B. Zeks, Mol. Cryst. Liq. Cryst. **263**, 61 (1995).
19. N.A. Clark, S.T. Lagerwall, Appl. Phys lett. **36**, 899 (1980).
20. T.P. Rieker, N.A. Clark, G.S. Smith, D.S. Parmar, E.B. Sirota, C.R. Safinya, Phys. Rev. Lett. **59**, 2658 (1987).
21. N.A. Clark, T.P. Rieker, J.E. Maclennan, Ferroelectric **85**, 79 (1988).
22. P.C. Willis, N.A. Clark, C.R. Safinya, Liq. Cryst. **11**, 581 (1992).
23. P.C. Willis, N.A. Clark, J.Z. Xue, C.R. Safinya, Liq. Cryst. **12**, 891 (1992).
24. N.A. Clark, T.P. Rieker, Phys. Rev A **37**, 1053 (1988).
25. J.E. Maclennan, N.A. Clark, M.A. Handschy, M.R. Meadows, Liq. Cryst. **7**, 753 (1990).
26. Z. Zhuang, A.G. Rappaport, N.A. Clark, Liq. Cryst. **15**, 417 (1993).
27. M. Nagakawa, T. Hakahane, J. Phys. Soc. Jpn. **55**, 4429 (1986).
28. M. Nagakawa, J. Phys. Soc. Jpn. **59**, 1995 (1990).
29. L. Limat, J. Prost, Liq. Cryst. **13**, 101 (1993).
30. A. De Meyere, H. Pauwels, E. De Ley, Liq. Cryst. **14**, 1269 (1993).
31. L. Limat, J. Phys. France II **5**, 803 (1995).
32. P. Gisse, J. Pavel, H.T. Nguyen, V.L. Lorman, Ferroelectrics **147**, 43 (1993).
33. P. Cluzeau, Thesis of University of Bordeaux I (France, 1995).
34. Y. Takanishi, K. Hiraoka, U.K. Agrawal, H. Takezoe, A. Fukuda, M. Matsushita, Jpn. J. Appl. Phys. **30**, 2023 (1991).
35. J. Prost, R. Bruinsma, Ferroelectrics **148**, 25 (1993).
36. Y. Takanishi, A. Ikeda, H. Takezoe, A. Fukuda, Phys. Rev. E **51**, 400 (1995).
37. V. Laux, N. Isaert, H.T. Nguyen, P. Cluzeau, C. Destrade, Ferroelectrics **179**, (1996), 25.
38. M.P. Cuminal-Sanchis, Thesis of University of Montpellier II (France, 1997).
39. P.S. Carvalho, P. Cluzeau, C. Destrade, H.T. Nguyen, M.R. Chaves, Ferroelectrics **178**, 195 (1995).
40. P. Cluzeau, J.C. Rouillon, H.T. Nguyen, M. Brunet, 7^{e} Colloque d'Expression Française sur les Cristaux Liquides (Sophia-Antipolis, 1995).
41. M. Brunet, L. Lejcek, Liquid Cryst. **19**, 1 (1995).